PCCP

Accepted Manuscript

This is an *Accepted Manuscript*, which has been through the Royal Society of Chemistry peer review process and has been accepted for publication.

Accepted Manuscripts are published online shortly after acceptance, before technical editing, formatting and proof reading. Using this free service, authors can make their results available to the community, in citable form, before we publish the edited article. We will replace this *Accepted Manuscript* with the edited and formatted *Advance Article* as soon as it is available.

You can find more information about *Accepted Manuscripts* in the **Information for Authors**.

ROYAL SOCIETY OF CHEMISTRY

www.rsc.org/pccp

Influence of intermolecular interactions on spectroscopic characteristics of metal nanoparticles and their composites

Igor I. Shaganov[1], Tatiana S. Perova[*2,3], Maria V. Mukhina[3], Irina V. Martynenko[3], Alexander V. Baranov[3], Anatoly V. Fedorov[3], Valerie Gerard[4], and Yuri K. Gun'ko[3,4]

[1]*Vavilov State Optical Institute, 199034, St.-Petersburg, Russia*

[2]*Department of Electronic and Electrical Engineering, Trinity College Dublin, Dublin 2, Ireland*

[3]*ITMO University, 49 Kronverskiy pr., Saint Petersburg, 197101, Russia*

[4]*School of Chemistry, Trinity College Dublin, Dublin 2, Ireland*

Abstract

In this paper we investigate the possibility to apply the concepts of non-specific intermolecular interactions and dispersive local field effect approach for study of influence of interactions of metal nanoparticles with matrix's molecules on spectral characteristics of composites. The effect of intermolecular (inter-particles) interactions and the influence of the dielectric environment on the peak position of the plasmon resonance band of colloidal solutions and thin films formed from noble metal nanostructures is determined. Simulated and experimental absorption spectra obtained for a colloidal solution of silver and gold nanoparticles, of various shapes and sizes in water and glycerol, are in good agreement.

----

[*]Author for correspondence: Tel.: +3531 8961432; FAX: +3531 677 2442; e-mail: perovat@tcd.ie

1. INTRODUCTION

The investigation of the optical properties of metal nanoparticles of different size and shape is currently attracting a great deal of attention from researchers. Excitation of surface plasmons in such particles has a huge practical interest for fabrication of different media with unique optical properties and devices based on them. Amongst potential applications are highly sensitive chemical and biological sensors, composite materials with negative dispersion and structures with extraordinary transmission etc. [1-6]. More recently small metal particles were also utilised in waveguides, lasing, surface-enhanced spectroscopy, photocatalysis, solar cells (or photovoltaic devices) and other areas of science and technology [7-11].

Since the optical properties of metal nanoparticles exhibit a notable dependence on their size [12,13], shape [14,15], volume concentration [16] as well as on the characteristics of the host matrix [17,18], this led to extensive exploration both theoretically and experimentally of several systems including, in particular, gold and silver nanostructures of different shapes in the form of a single particle, thin films and in colloidal solutions. This extensive research resulted in a number of text books, comprehensive reviews and detailed articles written on various methods of synthesis and fabrication of different composite systems as well as on modelling and characterisation of their linear (i.e. absorption, emission, luminescence, Raman scattering etc.) and nonlinear optical properties [1,3,4,7,19-22].

The modelling of optical properties of small particles is continuously developing. In particular, methods of calculations based on exact solutions of the Maxwell equations using Mie theory have been developed for a spherical particles (see, for example, textbooks [1,19,23]). In order to take into account the size and shape for non-spherical particles there are few approaches, namely using the modified Maxwell-Garnett approximation [22-24], the extended boundary condition method or surface integral approach (see review [25] and references therein) and various numerical calculations. The first method required to use certain approach for introducing a specific expression from Ref. [26] for the depolarization factor into the Maxwell-Garnett theory [27] in order to take into account the size and an arbitrary shape of small particles. The second approach was employed in Ref. [28] to calculate depolarisation factors in solids for the calculation of the absorption spectra of powders. It is important to note that both aforementioned techniques do not include retardation and therefore the techniques are restricted to smaller particles size only (quasistatic approximation), i.e. to only those particles with a radius much smaller than the corresponding surface plasmon resonance wave vector ($a<<\lambda/2\pi n$). However,

the advantage of both these techniques is that they drastically reduce the computational time of absorption spectra so that a very fine sampling of the electromagnetic properties can be achieved.

Numerical calculations that can be applied to the particles of a larger size and with virtually any shape, are well described in a number of comprehensive reviews (see, for example, Refs. [4,7,21,22]) and include an application of T-matrix, discrete dipole approximation (DDA), finite difference in the time domain (FDTD) and boundary element (BE) methods to colloids of metal particles. However, as was mentioned in Ref. [25], the results of experiments and numerical calculations, performed, for example, with DDA method, did not always match when the real particle shape based on TEM measurements is taken into account.

In this work, we applied the previously suggested method of dispersion of effective field (DEF) and conceptions of the theory of molecular spectroscopy [29-34] to analyse the effect of resonant and inductive-resonant dipole-dipole interactions on the plasmon absorption frequency of colloidal solutions of gold and silver nanoparticles, as well as of granular gold films.

The possibility of using the conceptions of spectroscopy of intermolecular interactions (IMI) for the study of the absorption spectra of metal nanoparticles was demonstrated using the example of the experimental investigation of the influence of the permittivity of dilute colloidal solutions of Au and Ag nanoparticles in water and in glycerol. It was shown that based on the model of dynamic polarization it is possible to use the results of the effective medium theory (Maxwell-Garnett, in particular) for modelling the absorption of metal particles whose dimensions do not satisfy the quasistatic approximation and whose shape significantly deviates from spherical.

2. THEORETICAL APPROACH

A simple phenomenological model for describing the spectral properties of the composite media was proposed in the early 20$^{\text{th}}$ century in Refs. [27]. In accordance with this model, the relationship between the optical properties of a metal and the corresponding metallic colloidal solution has the following form

$$\frac{\hat{\varepsilon}_c(v) - \varepsilon_h}{\hat{\varepsilon}_c(v) + 2\varepsilon_h} = \frac{f \cdot (\hat{\varepsilon}(v) - \varepsilon_h)}{\hat{\varepsilon}(v) + 2\varepsilon_h} \tag{1}$$

Here $\hat{\varepsilon}_c(v)$, ε_h and $\hat{\varepsilon}(v)$ are the dielectric permittivities of the composite medium, host matrix and metal embedded into a transparent matrix in the form of small size spherical particles, and f

4

is their concentration (or filling fraction). The effectiveness of this model has found ample evidence in the last decade [1,35]. At the same time, as was shown in Ref. [16], the Maxwell-Garnett theory describes the properties of a dilute colloidal solution of small spherical gold particles, which are characterized by the condition that the particle diameter is much smaller than the wavelength of the probing radiation, i.e. $d \ll \lambda$. As it turned out later, this condition is determined by the fulfilment of the quasistatic limit, for which, on the one hand, the particle size is greater than the mean free path of conduction electrons, and, on the other hand, it is small enough to not make a significant contribution to the radiation scattering. As suggested in Ref. [1] the size of such particles must satisfy to the condition $d < 0.01\lambda$. At the same time, as shown in Ref.[36] using an example of gold spherical particles in porous alumina matrix, a noticeable disagreement between experiment and theory is observed for particles with size smaller than 20 nm.

Later, the Maxwell-Garnett formula was modified and extended to the case of particles of ellipsoidal shape [34,37]

$$\frac{\hat{\varepsilon}_i(v) - \varepsilon_h}{L_i \hat{\varepsilon}_i(v) + (1 - L_i)\varepsilon_h} = \frac{f \cdot (\hat{\varepsilon}(v) - \varepsilon_h)}{L_i \hat{\varepsilon}(v) + (1 - L_i)\varepsilon_h} \quad . \quad (2)$$

Here $\hat{\varepsilon}_i(v)$ is the ith component of the dielectric permittivity tensor of composite, and L_i is a corresponding form-factor, defined as the ratio of the semi-axes of the model ellipsoid. For a sphere, $L_i = 1/3$ and expression (2) takes the usual form of the formula (1). Solving Eq. (2) with respect to $\hat{\varepsilon}_i(v)$, we can obtain the following expression [38,39]

$$\hat{\varepsilon}_i = \frac{f(\hat{\varepsilon}(v) - \varepsilon_h)\,\varepsilon_h\,(1 - L_i) + \varepsilon_h[L_i\hat{\varepsilon}(v) + (1 - L_i)\varepsilon_h]}{L_i\hat{\varepsilon}(v) + (1 - L_i)\varepsilon_h - f(\hat{\varepsilon}(v) - \varepsilon_h)L_i} \quad (3)$$

Separating the imaginary part of this expression, we obtain the dielectric loss spectrum of the composite

$$\varepsilon_{2i}^{comp}(v) = \text{Im}\,\hat{\varepsilon}_i(v) \quad (3a)$$

see for details Refs. [38,39]. This expression takes into account the inductive-resonant dipole-dipole interactions of the particles with the molecules of the environment, as well as the resonant dipole-dipole interactions between the particles themselves. For simplicity we will omit the term "dipole-dipole" and will further refer to these interactions just as "inductive-resonant" and "resonant" interactions, respectively. It should be noted that the latter is well taken into account only at volume concentrations of particles up to 0.3 [14]. In the case of highly diluted

composites, when the volume concentration of particles is less than 0.1 - 0.05 and the resonant dipole-dipole interactions are either absent or have little effect on the position of the bands of plasmon resonance absorption, the Eq. (3) can be greatly simplified. As was shown in Ref. [38], the corresponding expression for the dielectric loss spectrum of the composite becomes

$$\varepsilon_2^{comp}(v) = f\varepsilon_2(v)\theta(v) = f\varepsilon_2(v)\varepsilon_h^2\left[\varepsilon_h + L(\hat{\varepsilon}(v) - \varepsilon_h)\right]^{-2} \qquad (4)$$

where $\theta(v)$ is the correction factor accounting for the spectral difference between the effective microscopic $E_{eff}(v)$ and the average macroscopic $E_0(v)$ fields of the electromagnetic wave in condensed matter

$$\theta(v) = \varepsilon_h^2\left|\varepsilon_h(1-L) + L \cdot \hat{\varepsilon}(v)\right|^{-2}. \qquad (5)$$

It should be noted that Eqs. (3) – (5) refer to the case of composites when the ellipsoids, which model the shape of the impregnated particles, are oriented parallel or perpendicular to the direction of the electric field vector of the incident electromagnetic field. In case of the random orientation of the particles the effective dielectric loss spectrum of the composite is given by the following expression [38]

$$\varepsilon_2^{eff}(v) = \frac{1}{3}\sum_{L_i}\varepsilon_{2i}(v) \qquad (6)$$

where L_i are the values of form factors for the main axes of the ellipsoid.

As was shown in Ref. [38], the expressions (4) and (5) are the elaboration of method of dispersive effective field, utilised in the 60s-70s of the last century to establish a link between the observed absorption spectra of various condensed media and spectroscopic characteristics of microscopic oscillators (molecules) responsible for this absorption [29-31]. In fact, the effective field method allows the conversion from the spectrum of the bulk material to the spectrum of its microscopic counterpart. It was found that the differences between micro and macro properties of condensed matter are related to intermolecular interactions of the constituent molecules and particles, resulting in a spectral difference between the average and effective electromagnetic fields. DEF method in some cases provided a clear quantitative description of intermolecular interactions in liquids and solution as well as in crystalline media [33,39-42]. In particular, using this method, the authors of Refs.[29,42-45] were able to trace the influence of resonant and inductive-resonant interactions not only on the peak position but also on the intensity and shape [47,48] of the analysed absorption bands. It is worth noting that in this case the effective field E_{eff}

plays the role of the electrodynamic equivalent of the total action on molecule of the external macroscopic field and the field forces of the intermolecular interactions (IMI). External macroscopic field $E(v)$ is considered here as a weak perturbation and so this consideration does not extend beyond the linear molecular optics. In accordance with Refs.[29,40], spectroscopic characteristics of the molecule in a single-component solution or condensed medium are characterised by the spectrum of the Einstein coefficient $B(v)$, having the physical meaning of the spectral density of the quantum transition probability for the absorption and associated with the spectrum of the imaginary part of the condensed medium via the correction factor $\theta(v)$:

$$B(v) = \frac{2\pi \operatorname{Im} \hat{\varepsilon}(v)\theta(v)}{Nh} \qquad (7)$$

According to the Lorentz model, the correction factor $\theta(v)$ for isotropic homogeneous medium is given by

$$\theta(v) = \left| \frac{E(v)}{E_{eff}(v)} \right|^2 = \frac{9}{\left| \hat{\varepsilon}(v) + 2 \right|^2}, \qquad (8)$$

where $\hat{\varepsilon}(v) = \varepsilon_1(v) - i\varepsilon_2(v)$ represents the spectral variation of the complex dielectric constant of the medium within the range of the absorption band.

We note that the aforementioned equations can be applied not only to the individual molecules, but also to micro- and nano-particles. In this case, formula (7) can be conveniently represented in the following form [38]

$$\varepsilon_2^{mic}(v) = \varepsilon_2^{mac}(v) \cdot \theta(v), \qquad (9)$$

where $\varepsilon_2^{mic}(v)$ and $\varepsilon_2^{mac}(v)$ are the spectra of imaginary part of microscopic and macroscopic (bulk) dielectric permittivity of particle's material, respectively.

This conclusion is supported by the fact that in case of the lattice vibrations, the DEF method has demonstrated a good agreement between $B(v)$ and $\varepsilon_2^{mic}(v)$ spectra and intrinsic frequencies of the lattice vibrations, calculated from the elastic characteristics of the crystal [45,47].

When taking into account the local field effect using the Lorentz model, we are talking about the frequency of oscillation of the micro-regions of spherical shape in the crystal with dimensions much larger than the lattice constant, but much smaller than the wavelength of the probing

radiation. This can also be observed in other media. Therefore, we can conclude that the Eq. (9) corresponds to the spectrum of a single spheroidal particle, whose own spectral characteristics differ from that of the bulk. This type of particles can be considered as "meso-oscillators" or "mesoparticles" whose spectral properties in the long-wavelength limit ($d \ll \lambda$) do not depend on their size, and are due to the spectral differences of the macroscopic and microscopic electromagnetic fields. As already indicated, these differences are determined by the optical characteristics of the bulk material of absorbing particles as well as by parameters of the surrounding matrix. For isolated particles in a medium ε_h, the homogeneous field inside the ellipsoidal particles $E_{in}(v)$ and the electric field of the surrounding medium $E(v)$ are related by the following formula which, after considering a screening effect, can be expressed as in Ref. [49]:

$$\frac{E(v)}{E_{in}(v)} = \frac{\varepsilon(v) + k\varepsilon_h}{3\varepsilon_h},\tag{10}$$

where k is a screening parameter, related to the form factor L as follows

$$k = (1-L)/L .\tag{11}$$

It is easy to see that the Eq. (10) correlates with Eq.(5). The role of the local field in this case is to represent the average field inside the particle, and the acting field is a field in the surrounding medium. If $\varepsilon_h = 1$ and $L = 1/3$, the expression (10) takes the form characteristic for the Lorentz model, previously used in [29,33,40] for one-component condensed matter to calculate the microscopic characteristics of the constituent ions, molecules or clusters.

In accordance with the results of the theory of intermolecular interactions, the process of formation of the intense absorption bands during the transition from an isolated molecule (particle) to the condensed state of the corresponding medium (with peak position of absorption spectrum, v_{abs}) can be presented as:

$$v_{abs} = v_{intr} + \Delta v_{nonlin} + \Delta v_{res}\tag{12}$$

where v_{intr} is an intrinsic frequency of electronic or vibrational excitation of a molecule that does not interact with other molecules (or particles) of the environment at the considered excitation frequency. The second term in the right side of the Eq. (12), Δv_{nonlin}, describes the nonlinear changes in the properties of molecules under the influence of a strong electromagnetic field. This term reflects the presence of a so-called inner dielectric effect (Intrinsic effect) [1], accompanied by a change in the electronic levels and the band structure of the particle, and, in general,

changes in the ionization potential, the bonding energy, the crystalline structure and other parameters of the medium. The dependence of the above mentioned properties on the particle's sizes is often defined as a quantum-size effect. The third term of sum in Eqn. (12), Δv_{res}, reflects the manifestation of the dielectric effect (Extrinsic effect) [1], due to the contribution of the resonant dipole-dipole interactions of molecules (particles) at a frequency of considered excitation. The dielectric effect stated above is a consequence of the polarization of the medium as a response to an external electromagnetic field $E(v)$, considered as a weak perturbation. In this case, specifically, it is possible to establish a link between the optical constants of bulk material and the spectral properties of the microparticles or composites formed from it. As it is well known, the interaction potential of a molecule with the environment can only be obtained on the basis of models for the pair potentials of dispersion, induction and resonance interactions [40]. With respect to the resonant dipole-dipole interactions, this problem was considered in Refs.[41,50]. According to [41,50] the part of the resonant frequency shift of the ith isolated vibrations at $\Delta v \ll v_{intr}$ within the oscillator model and the dipole-dipole approximation is described by the following expression

$$\Delta v_{res} = \frac{N \left| \frac{d\mu}{dq} \right|^2}{6\pi c^2 v_{int\,r}}, \tag{13}$$

where N is the concentration of oscillators, and $\left| \frac{d\mu}{dq} \right|^2$ is a square of the matrix element of the transition dipole moment. At the same time the full dynamic frequency shift of the considered transition, due to the effect of the background polarization, increases and becomes equal to

$$\Delta v_{dyn} = \frac{N \left| \frac{d\mu}{dq} \right|^2 \left(\frac{\varepsilon_\infty + 2}{3} \right)}{6\pi c^2 v_{int\,r}}. \tag{14}$$

Thus it is obvious that the overall dynamic contribution of resonant interactions to the frequency maximum (or the peak position) of the spectrum for a condensed medium can be divided into two parts:

$$\Delta v_{dyn} = \Delta v_{res} + \Delta v_{backg} \tag{15}$$

We can assume that the difference between these shifts will be determined by the contribution of the background polarization, exhibiting the influence of all other energy levels of the system on

the considered transition. In the case of IR spectroscopy this shift reflects the presence of electron-phonon interactions in condensed media. In accordance with Eqs.(13) - (15), this contribution can be expressed as

$$\Delta v_{backg} = \Delta v_{dyn} - \Delta v_{res} = \frac{N \frac{(\varepsilon_\infty - 1)}{3} \left| \frac{d\mu}{dq} \right|^2}{6\pi c^2 v_{int\,r}} \qquad (16)$$

Obviously, this part of the shift is of the same nature as the inductive-resonant frequency shift of non-interacting absorbing impurity centres in a transparent matrix (or molecules in a dilute solution), reflecting the effect of the dielectric constant of the solvent through the reactive field acting on them in a non-absorbing medium. According to [32,51], this inductive-resonance shift is described by

$$\Delta v_{ind-res} = \left\{ \frac{(\varepsilon_0 - 1)}{(2\varepsilon_0 + 1)} \right\} \times \frac{\left| \frac{d\mu}{dq} \right|^2}{4\pi^2 c^2 v_{int\,r} r_{onz}^3} \cdot \qquad (17)$$

Here ε_o is the dielectric permittivity of the solvent, and $r_{onz.}$ is the Onsager's cavity radius of an absorbing molecule (see Refs. [11,52] for details). It can be shown that Eqs. (16) and (17) are similar. It should be noted that N in the Eq.(16) can be expressed by the so-called structure radius, R, of the medium-forming particles. If we assume that the particle volume is $V = 1 / N = 4/3\,\pi\,R^3$, where R is its structure radius, the Eq. (16) can be transformed to

$$\Delta v_{backg} = \frac{(\varepsilon_\infty - 1)}{6} \cdot \frac{\left| d\mu / dq \right|^2}{4\pi^2 c^2 v_{int\,r} R^3} \cdot \qquad (18)$$

Equations (14) and (16) can be easily expressed in terms of the dielectric loss spectrum of the condensed medium $\varepsilon_2(v)$. Bearing in mind that $\left| d\mu / dq \right|^2 = Fe^2/m$, and the oscillator's strength is determined as $F = \frac{2mv}{Ne^2} \int \varepsilon_2(v)\theta(v)dv$, we can expressed in accordance to [41,50] a total resonant dipole-dipole shift (or total shift, Δv_{tot}) of the frequency maximum of absorption band as

$$\Delta v_{tot} = \frac{1}{\pi(\varepsilon_\infty + 2)} \int \varepsilon_2(v)dv , \qquad (19)$$

while the expression (16) for the background contribution to the frequency shift can be reduced to the form

$$\Delta \nu_{backg} = \frac{(\varepsilon_\infty - 1)}{\pi(\varepsilon_\infty + 2)^2} \int \varepsilon_2(\nu) d\nu. \qquad (20)$$

If we assume as an approximation that the structural and Onsager's radii of molecules are close, then at equality of the background dielectric constants of the bulk material particles and of the matrix ε_∞ and ε_h, the background part of the frequency shift in the medium coincides with the inductive-resonant shift in dilute solution up to a coefficient of $(2\varepsilon_\infty + 1)/6$. This means that for the most common values of $\varepsilon_\infty = 2 - 3$, this mismatch does not exceed 20%. Nevertheless, the comparison of experimental and calculated results show that for the modelling of plasmon resonance of gold particles in different solutions the Eq. (18) provide better results than formula (17).

Therefore, considering all the above, with the exception of nonlinear effects, Eq. (12) can be rewritten as

$$\nu_{abs} = \nu_{intr} + \Delta\nu_{ind\text{-}res} + \Delta\nu_{res} \qquad (21)$$

It should be noted that at greater distances, d, between the particles (i.e. for $d \gg \lambda$ or for the filling factor $f \ll 1$), the resonant dipole-dipole interactions are negligible and the dominant role in the Eq. (21) is played by the inductive-resonant shift, reflecting the external manifestation of the dielectric effect in diluted composites.

Numerical analysis of the validity of this approach can be made on the basis of the previously mentioned approach of the dispersion of the internal field, allowing to trace separately the influence of individual parts of the potential IMI not only on the frequency maximum but also on the intensity and shape of the analysed absorption bands. The virtual spectrum $\varepsilon_2^{mic}(\nu)$, obtained at $\varepsilon_h = 1$ determines the own spectroscopic characteristics of the separate isolated particles (or molecules), since the transition from spectroscopic characteristics of the bulk material (from spectrum $\varepsilon_2(\nu)$) to spectrum $\varepsilon_2^{mic}(\nu)$ is equivalent to "disabling" the dynamic frequency shift, comprising the influence of purely resonant as well as inductive-resonant interactions. By doing this we obtain the spectrum of the isolated particles in vacuum.

We emphasize once again that Eqs. (20) - (21) are valid for the description of the spectroscopic micro-characteristics of not only molecules but also clusters. Thus we can also assume that Eqs. (4) and (5) at $f = 1$ in the long-wavelength limit describes the characteristics of individual micro-particles, which can be regarded as a kind of "mesomolecules" [53,38,39]. Note that when $f =$

0.02-0.01, corresponding to the diluted composite media, the results of calculations by Eqs. (4) and (5) almost totally coincide with a rigorous expression (3a). Based on the above it is obvious that for dilute colloidal solutions of metal particles, the contribution to the frequency shift of the plasmon by inductive-dipole interactions can be expressed as the difference between the frequency maximum of spectra $\varepsilon_2^{mic}(v)$, obtained at $\varepsilon_h = 1$ and at specific value ε_h of a particular matrix.

To illustrate this approach, in the next sections we show the capabilities of dispersive effective field and the theory of intermolecular interactions methods for the analysis of resonant and inductive-resonant interactions using the examples of the model oscillator spectrum, as well as spectra of gold colloids and granular films.

3. Results and Discussion

Spectroscopic Characteristics of Mesoparticles in Case of the Model Oscillator, Granular Films and Gold Colloids

To demonstrate the workability of the DEF method for the analysis of the influence of resonance and inductive-resonance interactions, we use first the isolated absorption band of a model oscillator with the following dispersion parameters: $v_t = 1000$ cm^{-1} , $\rho = 0.1$, $\gamma = 0.1$ and $\varepsilon_\infty = 3$ [44,47]. The frequencies of absorption spectra of bulk material and corresponding mesoparticles at $\varepsilon_h = 1$ and $\varepsilon_h = 3$ as well as resonance and inductive resonance frequency shifts are presented in Table 1.

As can be seem from Table 1, there is good agreement between resonant and inductive-resonant shifts of absorption bands, obtained from spectra $\varepsilon_2^{meso}(v)$ and using the analytical expressions (19) and (20) for Δv_{tot} and Δv_{backg}. It should be noted that in case of metal-dielectric composites the resonant dipole-dipole interactions are markedly manifested only when $f > 0.1$. At higher concentrations, they lead to a smearing of the plasmon absorption band and to its transition to the non-selective spectrum of a cermet. In these conditions the concepts of DEF method do not work. At the same time for the island-like granular films this method allows to demonstrate the important role of the resonant dipole-dipole interactions in the formation of their spectroscopic characteristics. An appropriate analysis of the influence of the resonant interactions on the frequency of gold plasmons by DEF can be performed based on the results obtained previously in Ref. [54]. The resonant frequecy shift of the plasmon oscillations of granular gold films using data of Ref. [54] are presented in Table 2. As can be seen from Table 2 there is a

reasonable agreement between the frequency shifts, Δv_{tot}, obtained by DEF method and analytical expression (19) for the resonant shift. For calculations of Δv_{tot} the Eq. (19) in a form of

$$\Delta v_{tot} = \frac{\sqrt{\langle\theta\rangle}}{3\pi} \int \varepsilon_2(v) dv$$ have been used, where $\langle\theta\rangle$ is the average of the local field correction

factor determined by the background dielectric constant of the medium in this spectral range. Note that the $\langle\theta\rangle$ values were calculated from the ratio of the integrated intensities of the corrected and the experimentally observed absorption bands $\langle\theta\rangle = \int \varepsilon_2(v)\theta(v) dv / \int \varepsilon_2(v) dv$ (see Ref. [43]). A considerable discrepancy in the compared data is obtained only for the very thin samples, while in other cases it does not exceed 10%. This discrepancy is obviously related to the errors in determination of the integrated intensities of the absorption bands, which are more significant in the case of the weaker absorption bands.

Analysis of the impact of the inductive-resonant dipole-dipole interactions on the frequency of plasmon resonance by the DEF method, was performed using the values of the optical constants obtained in Ref. [55]. The corresponding calculations are summarized in Table 3. We note again that in this calculation the plasmon frequency is totally independent from the value of the filling factor. At $f = 1$ the absorption bands obtained are related to the dielectric loss spectrum of a single particle in an appropriate medium of ε_h. At $f = 0.01$ the frequency maximum of bands will not change, and the spectra themselves, characterizing in this case the spectra of dilute composite, practically coincide with the spectra obtained by the rigorous expression [3]. The magnitude of induction-dipole shift is then determined from the relation

$$\Delta v_{ind-res} = v(\varepsilon_h=1) - v(\varepsilon_h).$$

Analysis of the obtained data shows that for the analytical evaluation of inductive-resonant interactions in this case, a more suitable expression is Eq. (18), wherein the role of the background component of the permittivity ε_∞ performs by the ε_h of the environment. In accordance with Eq. (18), the inductive-resonant shifts must, on the one hand be determined by the oscillator strength of mesoparticle, and on the other hand, increase linearly with increasing values of ε_h in agreement with the change in the dielectric multiplier $D = (\varepsilon_h -1)/6$. This dependence is presented in Fig. 1.

Using the above expression for D, we can simplify the Eq. (18) to the form $\Delta v = A \cdot D$, where A $\propto |d\mu / dq|^2$, i.e. A is proportional to the oscillator strength of plasmon in the considered here case. As can be seen from Table 3, the value $A = \Delta v/D$ does not depend on the nature of

13

mesoparticle's environment and deviates from the average value (A_{av} = 4715 cm^{-1}) by less than 10%.

In summary, although the results above apply to spherical particles, they appear to have wider applicability. Concepts from molecular spectroscopy can be applied to the absorption spectra of microparticles (or nanoparticles) and clusters, as well as to the analysis of purely molecular spectra.

Accounting for the Size and Shape of Gold and Silver Mesoparticles in the Calculation of the Spectral Characteristics $\varepsilon_2^{meso}(\nu)$ of Colloidal Solutions.

a) Theoretical background

Further development of the effective theory medium was possible using the model of so-called dynamic polarisation of the medium, that allowed to take into account not only the shape but also the real size of the modelled mesoparticle [23,26,56]. In this work the model of the dynamic polarisation was applied to the modelling of spectral characteristic of metal nanoparticles with shape far different from the spherical. In accordance with this model, Eq. (1), connecting the spectral characteristics of bulk metal and metal particles in colloid solution, takes the following form

$$\frac{\hat{\varepsilon}_i(\nu) - \varepsilon_h}{\hat{\varepsilon}_i(\nu) + k\varepsilon_h} = f\frac{\hat{\varepsilon}(\nu) - \varepsilon_h}{\hat{\varepsilon}(\nu) + k\varepsilon_h},\tag{22}$$

where k is a screening parameter.

Solving the Eq. (22) with respect to $\hat{\varepsilon}_i(\nu)$, we obtained a more useful form:

$$\hat{\varepsilon}_i(\nu) = \varepsilon_h\frac{fk(\hat{\varepsilon}(\nu) - \varepsilon_h) + \hat{\varepsilon}(\nu) + k\varepsilon_h}{\hat{\varepsilon}(\nu) + k\varepsilon_h - f(\hat{\varepsilon}(\nu) - \varepsilon_h)}.\tag{23}$$

As can be seen from Eq, (23) in this case we use a screening parameter k, which is related to the depolarisation coefficient, q, by the following expression [23,26,56]

$$k = \frac{1 - q}{q}.\tag{24}$$

The Eq. (24) looks very similar to the Eq.(11), in which the form-factor L is defined in quasistatic approximation. However, the depolarisation coefficient q in Eq. (24) is more complex

and, in accordance with the Eq. (25), enables to take into account not only the shape but also the particle size [23,26,56]:

$$q_i = L_i - L_i k^2 b_z^2 - \frac{2}{3} i L_i k^3 b_z^3 . \tag{25}$$

Here $k = \dfrac{2\pi n_h}{\lambda}$, where n_h is the refractive index of the medium, λ is the wavelength, b_z is the length of the particle along the optical axis for which the conditions of the dielectric confinement are realized. Therefore, the first term in Eq. (25) takes into account the shape of the particle, while the second term takes into account the dynamic polarisation, which appeared if the particle size does not satisfy the conditions of the quasi-static approximation and its response depends on the incident light phase. The third term in Eq. (25) accounts for the damping of the induced dipole moment.

For modelling of the particle shape, we use expressions similar to the ones used in Refs. [38,39]. For that we model the particle as an ellipsoid of revolution with the form factor $L_i = L_z$ for the long axis and $L_i = L_x = L_y$ for the short axes. In accordance with Refs. [57,39],

$$L_z = \frac{1}{1-p^2}\left[1 - p\frac{\arcsin(\sqrt{1-p^2})}{\sqrt{1-p^2}}\right], \tag{26}$$

$$\text{and} \qquad L_{x,y} = \frac{1-L_z}{2}, \tag{27}$$

where p is the ratio of particle size along the axis of revolution, b_z, to its size along the perpendicular axes, $b_{x,y}$. Such presentation allows to account for any type of particle confinement. In the case of nanowires, diameter of nanoparticle determined from Transmission Electron Microscopy (TEM) images is used as parameter b_z, and the ratio of the length to particle diameter, p, is assumed to be 1000. Nanoprisms and nanoboxes are described as oblate ellipsoids. Height of the particle triangular face is determined from TEM images and used as parameter b_z. Parameter p is calculated as the ratio of the height to the length of the perpendicular axis of nanoparticle, which is also determined from TEM images. In the case of spherical nanoparticles, its diameter also determined from TEM images is used as parameter b_z, and parameter p, is assumed to be 1. All sizes determined from TEM images are shown in Table 4 and obtained as the average size of more than 100 particles.

For calculations of dielectric loss spectra $\varepsilon_2^{meso}(v)$ of metal particles of different shapes and sizes, the spectrum of the imaginary part, $\mathrm{Im}(\hat{\varepsilon}_i(v))$ was found, taking into account the Eq. (25). The calculation of all three form-factors of micro-particles at their random orientation was performed using Eq. (28), where the resulting expression for $\varepsilon_2^{meso}(v)$ has the tensor form:

$$\varepsilon_2^{meso}(v) = \sum_i \varepsilon_{2i}, \tag{28}$$

where ε_{2i} is the imaginary part of $\hat{\varepsilon}_i(v)$. Here the summation is carried out on all three symmetry axes of the ellipsoid $i=x,y,z$.

Based on these theoretical considerations we performed the calculations of absorption spectra of gold and silver nanoparticles with and without accounting for shape and size of the particles. These calculations were performed by equalizing the corresponding component of tensor of dielectric permeability to unity.

б) Experiments and calculations

In this section we present the dependence of the spectral shift that occurs when the refractive index of the host matrix, the size, shape and the conditions of dielectric confinement of metal particles are changed.

Sample preparation and characterisation

For investigation of spectroscopic characteristics (i.e. absorption spectra) a number of samples of anisotropic metal nanoparticles (such as silver nanoprisms of various sizes, silver-gold nanoboxes, gold spherical nanoparticles and silver nanowires) were prepared. The colloidal solutions from some of the particles were prepared at volume concentrations of around 0.05 using solvents with different refractive indices, namely water ($n = 1.333$) and glycerol ($n = 1.473$). The absorption spectra were measured using spectrophotometer Cary 50 UV-Vis (Varian) and photometric cuvettes with thickness of 10 mm.

Synthesis of spherical gold nanoparticles: A 6mL aqueous solution of 1mM $HAuCl_4$ was brought to the boil, before the addition of 1mL of a 25 mM trisodium citrate solution. The reaction mixture was stirred under heating for 10 min, until it turned ruby red [58].

Synthesis of silver nanoprisms (AgNP) and gold/silver nanoboxes (AuNB): Silver seeds were produced by the addition of 5 mL of $AgNO_3$ (0.5 mM) at a rate of 2 mL/min to a solution

containing 5 mL TSC (2.5 mM), 250 µL PSSS (500 mg/L) and 300 µL NaBH$_4$ (10 mM). To produce AgNP, a volume of these comprised in the range of 100-250 µL wasdiluted in 10 mL of Millipore water to which were added 150 µL of ascorbic acid (10 mM) and 6 mL of AgNO$_3$ (0.5 mM) at a rate of 4 mL/min. 5 mL of TSC (25 mM) were finally added. Various sizes of AgNP were obtained by varying the amount of seeds used [59]. AuNB were formed by adding 1 mL of ascorbic acid (10 mM) to one 8 mL-batch of silver nanoprisms, followed by 10 mL of HAuCl$_4$ (0.5 mM) at the rate of 1 mL/min [60].

Synthesis of silver nanowires: Silver seeds were formed by adding 0.5 mL of a 6.10^{-4}M solution of AgNO$_3$ in ethylene glycol to 6 mL of ethylene glycol heated to 150°C. Subsequently, 6 mL of ethylene glycol solution containing 0.07 mol.L^{-1} of polyvinylpyrrolidone (PVP, monomer concentration) and 0.05 mol.L^{-1} of AgNO3 were added to the hot seed solution and stirred for an hour [61].

The nanoparticles were imaged by transmission electron microscopy (TEM) which allowed determining their shape and average size (see Figs. 2-5). AgNPs appeared fairly irregular in shape, from triangles to discs, although they were all flat, plate-like structures. AuNBs mostly retained the original triangular shape even though some were rounded. Table 4 presents the morphological characteristics of each type of nanoparticles.

Transfer of nanoparticles from water to glycerol was performed by centrifuging at 10,000 rpm for 30 min, removing the aqueous supernatant and replacing with glycerol. Dilute solutions with concentration of ~ 0.05 were prepared for the optical measurements, allowing to assume the absence of resonance interactions between metal particles. As was mentioned above, the size of nanoparticles for spectra simulations (as described in Section II.a.) was deduced from TEM images, examples of which are shown in Figs.2-4 (right panels), and summarized in Table 4.

The absorption spectra of silver nanoprisms of different sizes (26, 20 and 13.8 nm in height) diluted in water and glycerol to a concentration of ~ 0.05 are shown in Figs. 2b, 2d, 2f, while spectra of silver nanowires (of similar concentration) with diameter of 15.8 nm are shown in Fig. 3b. As can be seen from Figs. 2b, 2d, 2f, the peak position (frequency maximum) of absorption spectra is red-shifted with increasing particle size as well as with increasing refractive index (or $\varepsilon_h = (n_h)^2$) of the host matrix. These results are in agreement with published data on absorption of Ag nanoprisms of different sizes and diluted in number of different solutions (see, for example, Refs. [4,18,21]). We note that in our spectra registered up to 300 nm, the weak sharp peak is also

observed at ~ 335 nm, and weak peaks are seen at ~ 410 and 430 cm^{-1}. As was discussed in Ref. [4] based on polarised absorption measurements, the long wavelength peak (appeared in the region 500-800 nm, depending on the size of nanoprisms and, specifically, on the snip size) was assigned to the in-plane dipole-plasmon resonance, the weaker peak at ~ 460 nm to in-plane quadruple resonance, a small peak at 340 nm was identified as the out-of-plane quadruple, and a weak shoulder at 410 nm was assigned to out-of-plane dipolar resonance. The latter is normally barely resolved in non-polarised Ag nanoprisms spectra.

Spectra of Ag nanowires diluted in water and glycerol are shown in Fig. 3b. The spectrum demonstrated the main peak at ~ 400 nm and a shoulder at ~ 360 nm at the lower wavelength range. We note that Ag nanowires with different aspect ratio were investigated in our previous paper [62] where a significant distribution of plasmon peak position was demonstrated. Here, again it was demonstrated that the main peak position is red shifted with increase of the ε_h (from water to glycerol).

The absorption spectra of Au nanoboxes (with size of 64 nm) and nanospheres (with diameter of 2.5 nm) are shown in Figs. 4b and 4d. We must note that although some procedures for gold nanoprisms fabrication have been published for the last decade (see, for example, Refs. [15,63-65] investigation of their optical properties is still rather rare [15,65]. In absorption spectra of Au nanoboxes (Fig. 4b) we observed the main wide peak at ~724 nm (in water) and at ~ 760 nm (in glycerol) and the weak shoulder located at ~560 nm. The low-energy band is rather broad due to the polydispersity. We assigned this band to the dipolar modes, since the sizes of investigated here nanoparticles are relatively small. The high energy band (at ~ 560 nm) reflects the presence of some amount of spheres with diameter of similar size. The separation of these two types of particles is practically impossible and for this reason the optical spectrum of colloids shows two distinct plasmon bands. To compare with the results of Ref. [63] the intensity of 560 nm band is much lower and looks more like a shoulder which is probably due to the lower number of spheres-like nanoparticles present in our samples. The spectrum is red-shifted to compare with spectrum of Ref. [63] due to a smaller particles size in our case.

The experimental results along with the results of calculations of expected peak position of absorption spectra of corresponding nanoparticles in a specific solvent are summarized in Tables 5-8. As was expected, the size and shape of metal nanoparticles significantly influenced the peak position of the observed plasmon absorption band. This can be seen on the example of peak position of silver nanoprisms of different size presented in Table 5. In both host matrixes (water

18

and glycerol) we observed a significant red shift of peak position of absorption spectra with increase of the particle size. Surprisingly, the trends discovered earlier within the framework of concepts of spectroscopy of IMI, are also demonstrated in the case of silver particles of different sizes. As was expected, the best agreement is observed for the smallest investigated nanoparticles.

Unfortunately we did not have data on peak position of silver plasmon for the isolated particle, however we can compare the relative contribution of inductive-dipole interactions for replacement ε_h from ε_h =1.777 to ε_h= 2.17. The average value of $A = \Delta v/D$, obtained with accuracy of 10% for the silver from DEF method and the theory of IMI, is $A = 14990$ см$^{-1}$. The difference of the inductive-dipole shifts in glycerol and water can be estimated from the formula

$$\Delta v = A \cdot (D_{glyc} - D_{water}) \tag{29}$$

In case of the silver, this difference is equal to 982 cm^{-1}, which is in reasonable agreement with experimental value of 1012 cm^{-1} obtained for the particle with size of 13.8 nm ($\Delta v = 1012$ cm^{-1}) and 20.6 nm (($\Delta v = 1000$ cm^{-1}) and slightly less good for the larger particles (23 nm), for which the experimental value for Δv is 1142 cm^{-1} (see Table 5). A similar situation is reached in the analysis of inductive-resonant shifts of the nanowire particles. In case of Au nanoboxes, we obtain only semi-quantitative agreement between the experimental and calculated data on the relative frequency shifts (see Table 7).

This can be explained by a relatively large error in the modeling of the relative shift of absorption bands in considered dielectric matrixes, which arises due to the more complex shape of the particles. The estimation of the optimal modeling of shape of model particles is therefore complicated (see Table 7). Somewhere better results were obtained in case of gold particles of small size, listed in Table 8.

Here we need to explain that the formulas for the shift (resonant and inductive-resonant) are obtained for wavenumbers and, therefore, below we will use the value of the peak position, v, in absolute wavenumber units, and shifts of the peak positions as Δv. If we assume that the absorption from a single gold particle in the air occurs at λ =516 nm (or at 19380 cm^{-1}), as determine in Ref. [66], then the inductive-resonance shift is equal to $\Delta v = 19380 - 18692 = 688$ cm^{-1} for water, and to $\Delta v = 19380 - 18484 = 896$ cm^{-1} for glycerol. The relative shift can then be estimated as $\Delta v = 896 - 688 = 208$ cm^{-1}, which satisfactory agrees with the value of $\Delta v = 300$ cm^{-1}, calculated using Eq.(29) at A = 4717 cm^{-1} estimated in the previous section, and with $\Delta v = 246$

cm^{-1} obtained from experimental data of Ref. [66] (see Table 8). Thus our results show that the account of the real sizes of metal particles of complicated shape using the model of the dynamic polarisation allows to significantly improve the possibility of numerical modelling of influence of dielectric permeability of the environment medium on spectroscopic characteristics of investigated metal nanoparticles.

If we compare the results of Tables 5-8, we can see that the best agreement between experimental and calculated data is obtained for Ag nanorods. This is due to the fact the modelling the particle by prolate spheroid is better fit to the real shape in this case. However, bearing in mind the polydispersity of experimental spectra for nanoprisms and nanoboxes, which results in much wider experimental spectrum, we can conclude that in general the agreement between experimental and calculated spectra is reasonable in all considered cases.

4. CONCLUSIONS

To conclude, we applied the previously suggested DEF method of dispersion of effective field and conceptions of the theory of molecular spectroscopy to analyse the effect of resonant and inductive-resonant dipole-dipole interactions on the plasmon absorption frequency of colloidal solutions of gold and silver nanoparticles, as well as of granular gold films. One of the important issues during these calculations aroused as being the task of the adequate determination of the form-factor of particles, which may be significantly different from spherical. Despite the fact that the DEF method and the concepts of molecular spectroscopy considered here mainly refer to the case of spherical particles, a satisfactory agreement in the assessment of the relative magnitude of the inductive-dipole interactions performed on their basis and observed experimentally, pointed out to the generality of the law of manifestations of intermolecular interactions as in pure molecular spectra as well as in absorption spectra of metal micro- and nanoparticles and diluted colloidal systems. Since the account for the dynamic polarisation in accordance with expressions (24) and (25) can be carried out within the framework of formation of the standard correction factor $\theta(v)$ in dispersive effective field method, the use of the latter in the simulation of absorption spectra of metal particles whose size is beyond the scope of the feasibility of the quasistatic approximation, could be quite well-grounded and useful.

20

REFERENCES:

1. U. Kreibig, and M. Vollmer, *Optical Properties of Metal Clasters*; Springer-Verlag: Berlib, 1996.
2. C.M. Soukoulis, S. Linden, and M. Wegener, *Science,* 2007, **315**, 47-49.
3. L.M. Liz-Marzan, *Langmuir,* 2006, **22**, 32.
4. K.L. Kelly, E. Coronado, L.L. Zhao, and G.C. Schatz, *J. Phys Chem.* B 2003, **107**, 668.
5. P.K. Jain, X. Huang, I.H. El-Saed, and M.A. El-Saed, *Acc. Chem. Res.* 2008, **41**, 1578-1586.
6. T.W. Ebbesen, H.J. Lezec, H.F. Ghaemi, T. Thio and P.A.Wolff, *Nature*, 1998, **391**, 667-669.
7. F.J. Garcia de Abajo, *Rev. Mod. Phys.* 2007, **79**, 1267.
8. M. Moskovits, *Rev. Mod. Phys.* 1985, **57**, 783-826.
9. D. Franzke, A.J. Wokaun, *J. Phys. Chem.* 1992, **96,** 6377-6381.
10. G. A. Niklasson, *Sol. Ener. Mater.* 1988, **17**, 217-226.
11. K. Dolgaleva, and R.W. Boyd, *Adv. Opt. Photon.* 2012, **4**, 1-77.
12. K. M. Mayer, J. H. Hafner, *Chem. Rev.* 2011, **111**, 3828−3857.
13. M. El-Sayed, *Acc. Chem. Res*., 2001, **34**, 257-264.
14. G.V. Hartland, *Ann. Rev. Phys. Chem*. 2006, **57,** 403-430.
15. J. E. Millstone, S. Park, K. L. Shuford, L. Qin, G. C. Schatz, C.A. Mirkin, *J. Am. Chem. Soc.* 2005, **127**, 5312−5313.
16. T. Ung, L.M. Liz-Marzán, and P. Mulvaney, *J. Phys .Chem. B* 2001, **105**, 3441-3452.
17. C. Novo, A. M. Funston, I. Pastoriza-Santos, L. M. Liz-Marzan, P. Mulvaney, *J. Phys. Chem. C* 2007, **112**, 3−7.
18. L.J. Sherry, R. Jin, C.A. Mirkin, G.C. Schatz, R. P. Van Duyne, *Nano Lett.* 2006, **6**, 2060–2065.
19. C.F. Bohren, and D.R. Huffman, *Absorbtion and Scattering of Light by Small Particles*; Wiley: New York, 1983.
20. J. Perez-Juste, I. Pastoriza-Santos, L.M. Liz-Marzan, P. Mulvaney, *Coor. Chem. Rev*., 2005, **249,** 1870-1901.
21. I. Pastoriza-Santos, L.M. Liz-Marzan, *J. Mater. Chem*. 2008, **18**, 1724-1737.

22. V. Myroshnychenko, J. Rodriguez-Fernandez, I. Pastoriza-Santos, A.M. Funston, C. Novo, P. Mulvaney, L.M. Liz-Marzan, F.J. Garcia de Abajo, *Chem. Soc. Rev.* 2008, **37**, 1792-1805.

23. C.A. Foss Jr, G.L. Hornyak, J.A. Stockert, and C.R. Martin, *J. Phys. Chem.* 1994, **98**, 2963-2971.

24. V.M. Shalaev, *Physics Reports*, 1996, **272**, 61-137.

25. C. Pecharroman, J. Perez-Juste, G. Mata-Osoro, L.M. Liz-Marzan, P. Mulvaney, *Phys. Rev. B* 2008, **77**, 035418-1/7.

26. M. Meier, and A. Wokaun, *Optics Lett.* 1983, **8**, 581-583.

27. J.C. Maxwell-Garnett, *Philos. Trans. R. Soc. London* A **1904**, *203*, 385-420; *Philos. Trans. R. Soc. London* A 1906, **205**, 237-288.

28. R. Fuchs, *Phys.Rev.B* 1975, **11**, 1732.

29. N. G. Bakhshiev, O. P. Girin, V.S. Libov, *Sov.Phys.Dokl.* 1962, **145**, 1025-1027; *Sov. Opt. & Spectr.* 1963, **14**, 745-750.

30. A. A. Clifford, B. Crawford, *J. Phys. Chem.* 1966*, *70**, 1536-1543.

31. D.S. Chemla, and D.A.B. Miller, *Opt. Lett.* 1986, **11**, 522-524.

32. V. S. Libov, *Rus. J. Phys. Chem.* 1980, **54**, 817.

33. T.S. Perova, I.I. Shaganov, V.S. Libov, *Opt.& Spectroscopy* (USA), 1977, **42**, 524-527. Transl. of: *Opt.& Spektr.* (USSR), 1977, **42**, 883-888.

34. D.E. Aspnes, *Amer. J. Phys.* 1982, **50**, 704-708.

35. A. Moores, E. Goenttmann, *New J. Chem.* 2006, **30**, 1121-1132.

36. G.L. Hornyak, C.J. Patrissi, and C.R. Martin, *J. Phys. Chem. B* 1997**, 101**, 1548-1555**.**

37. R.W. Cohen, G.D. Cody, M. D. Coutts, B. Abeles, *Phys Rev. B* 1973, **8**, 3689-3701.

38. I. Shaganov, T. Perova, V. Melnikov, S. Dyakov, K. Berwick, *J. Phys. Chem.* C 2010, **114**, 16071-16081.

39. T. Perova, I. Shaganov and K. Berwick, Chapter XX in book *"Fourier Transforms – Approach to Scientific Principles";* Ed. G.S. Nicolić, Intech: Rijeka, Croatia, 2011, pp. 405-426.

40. N. G. Backhshiev, *Photophysics of Dipole-Dipole Interactions: Solvation Processes and Complex Formation*; St.-Petersburg University Press, St.-Petersburg, 2005, 500 p. (in Russian).

41. I.I. Shaganov, and V.S. Libov, *Fizika Tverdogo Tela,* (*Rus. Physics of Solid State)*, 1975, **17**, 1749-1752.

42. I.I. Shaganov, *Sov. J. Opt. Technol.*, 1992, **59**, 1-11.

43. I.I. Shaganov, T.S. Perova, R.A Moore, and K. Berwick, *J. Phys. Chem. B* 2009, **109**, 9885-9891.

44. I.I. Shaganov, T.S. Perova, K. Berwick, A. Moore, *Proc. SPIE***,** 2003, **4876**, 1158-1168.

45. T.S. Tolstykh (Perova), I.I. Shaganov, V.S. Libov, *Sov. Phys. Solid State* 1974, **16**, 657-662.

46. T.S. Perova, V. A. Melnikov, I. I. Shaganov, *Chem. Phys. Lett.* 2009, **479**, 81-85.

47. T.S. Perova, I.I. Shaganov, S. Unnikrishnan, and R.A. Moore, Spectroscopic Characteristics of Nano-Composite Structures in 3D, 2D and 1D Size Confinement, *Proceedings SPIE*, 2005, **5826**, 387-396.

48. T.S. Perova, I.I. Shaganov, J.K. Vij, O.F. Nielsen, P.A. Perov, *Assian Chem. Lett.*, 2000, **4**, 191-199.

49. J.A. Stratton, *Electromagnetic Theory*, MCr Hill, N-Y. 1941, p.212-215.

50. R. Frech, and J.C. Decius, *J. Chem. Phys.*, 1971, **54**, 2374-2380.

51. N.S. Bayliss, *J. Chem. Phys.* 1950, **18**, 292-296.

52. C.I.F. Bőttcher *Theory of Electric Polarisation*, 1952, Elsevier, Amsterdam

53. A. V. Ghiner, and G. I. Surdutovich, *Phys. Rev. A* 1994, **50**, 714-723.

54. I.I. Shaganov, *Rus. Opt.& Spectr.,* 1980, **49**, 181-184.

55. P.B. Johnson, and R.W. Christy, *Phys. Rev. B* 1972, **6**, 4370-4379.

56. E.J. Zeman, and G.C. Schatz, *J. Phys. Chem.,* 1987, **91**, 634-643.

57. J.A. Osborn, *Phys. Rev.* 1945, **67**, 351-353.

58. G. Frens, *Nat.-Phys. Sci.* 1973, **241**, 20-22

59. D. Aherne, D. E. Charles, M. E. Brennan-Fournet, J.M. Kelly, Y. K. Gun'ko, *Langmuir,* 2009, **25**, No.17, 10165-10173.

60. D. Aherne, M. Gara, J. M. Kelly, Y. K. Gun'ko,. *Func. Mater.*, 2010, **20**, 1329-1338.

61. Y. Sun, Y. Xia, *Adv. Mater.*, 2002, **14**, 833–837.

62. D.E. Charles, D. Aherne, M. Gara, M. Ledwith, Yu.K. Gun'ko, J.M. Kelly, W.J. Blau, M.E. Brennan-Fournet, *ACS Nano*, 2010, **4**, 55-64.

63. N. Malikova, I. Pastoriza-Santos, M. Schierhorn, N. A. Kotov, L. M. Liz-Marzan,. *Langmuir* 2002, **18,** 3694.

64. F. Kim, S. Connor, H. Song, T. Kuykendall, P. Yang, *Angew. Chem., Int. Ed.* 2004, **43**, 3673-3677.

65. S.S. Shankar, A. Rai, B. Ankamwar, A. Singh, A. Ahmad, M. Sastry, *Nature Mater.* 2004, **3**, 482-488.

66. T. Okamoto, T. Yamaguchi T. Kobayashi, *Opt. Letters*, 2000, **25**, 372-374.

67.

Table 1. Calculated and experimental frequency shifts of absorption band of model medium on transition from the bulk materials to spherical mesoparticles at condition of quasistatic approximation at $d << \lambda$.

ν_{max}, cm^{-1}		$\Delta\nu$ from DEF method		$\Delta\nu$ from IMI method	
Spectrum $\varepsilon_2(\nu)$	Spectrum $\varepsilon_2(\nu)\theta(\nu)$	$\Delta\nu_{tot}$, cm^{-1} from spectra	$\Delta\nu_{ind-res}$, cm^{-1} from spectra	$\Delta\nu_{tot}$, cm^{-1} Eq. (19)	$\Delta\nu_{backg}$, cm^{-1} Eq. (20)
1000	1117 (ε_h =1) 1067 (ε_h = 3)	117 67	117-67= 50	118	47

Table 2. Resonant shifts of frequency of plasmon vibrations in granular gold films estimated from data of Ref. [22].

Thick-ness	Experimental spectrum $\varepsilon_2(\nu)$			Spectrum $\varepsilon_2^{mic}(\lambda) = \int \varepsilon_2(\lambda)\theta(\lambda)d(\lambda)$				Calculation Eq. (19)
d, nm	λ_{max}, nm	ν_{max}, cm^{-1}	$\varepsilon_2(\nu)$ x 10^{-3}	λ_{max}, nm	$\varepsilon_2^{mic}(\lambda)$x 10^{-3}	$\langle\theta\rangle$	$\Delta\nu_{tot}$,* cm^{-1}	$\Delta\nu_{tot}$, cm^{-1}
5.5	571	17513	1.4	529	0.49	0.393	1390	1840
7	593	16863	2.1	540	0.5	0.238	2040	2360
8.5	604	16556	2.7	528	0.53	0.196	2347	2600
11	639	15649	4	525	0.52	0.13	3254	3200
16	646	15480	4.4	527	0.53	0.12	3423	3320
21	654	15290	5.2	528	0.526	0.101	3613	3620

*These values obtain as a difference of $\Delta\nu_{tot} = \nu_{av} - \nu_{max}$, where ν_{av} = 18903 cm^{-1} corresponds to the average maximum wavelength (λ_{max}) of spectra $\varepsilon_2^{mic}(\lambda)$, listed in column 5.

Table 3. Inductive-resonant shifts of frequencies of isolated plasmons of gold, obtained by the DEF method and considerations of the theory of intermolecular interactions (calculations using Eq. (4) at $L = 1/3$).

ε_h	λ max, nm	ν, cm^{-1}	$\Delta\nu_{ind\text{-}res}$, cm^{-1}	$D = (\varepsilon h - 1)/6$	$\Delta\nu / D$
1	508	19700	0	0	0
2	526	19000	700	0.1667	4200
3	554	1650	1650	0.3333	4950
4	581	17200	2500	0.5	5000
6	635	15750	3950	0.833	4740
9	740	13450	6250	1.333	4687

Table 4. Characteristic sizes of metal nanoparticles determined from TEM images.

	Nanowires	Spherical nanoparticles	Nanoboxes	Nanoprisms	
Diameter (nm)	15.8	2.5	-	-	
Length (nm)	> 10000	-	-	-	
Height of the triangle face (nm)	-	-	64	126a	23
				126b	20.6
				126f	13.8
Length of the axis perpendicular to the triangle face (nm)	-	-	3.4	126a	1.3
				126b	1.1
				126f	1

Table 5. Calculated and experimental value obtained for the peak position of spectra $\varepsilon_2^{meso}(\nu)$ for Ag nanoprisms of different size impregnated into two different matrices (water (W) and glycerol (G)).

Matrix	Name	Size	Calcu-lation, shape λ_{max}, nm	Calcu-lation, shape+size λ_{max}, nm (ν_{max}, cm^{-1})	Measurement λ_{max}, nm (ν_{max}, cm^{-1})	Difference Calc. $\Delta\lambda(_{G-W})$, nm $\Delta\nu(_{G-W})$, cm^{-1}	Difference Meas. $\Delta\lambda(_{G-W})$, nm $\Delta\nu(_{G-W})$, cm^{-1}
Water (W)	126a	23	486	580 (17241)	579 (17271)		
	126b	20.6		551 (18149)	550 (18182)		
	126f	13.8		495 (20202)	494 (20243)		
Glycerol (G)	126a	23	519	632 (15823)	620 (16129)	52 (1418)	41 (1142)
	126b	20.6		594 (16835)	582 (17182)	43 (1314)	32 (1000)
	126f	13.8		532 (18797)	520 (19231)	37 (1405)	26 (1012)

Table 6. Calculated and experimental value obtained for the peak position of spectra $\varepsilon_2^{meso}(\nu)$ for Ag nanowires (with diameter of 15.8 nm) impregnated into water and glycerol.

Matrix	Calculations		Measurement λ_{max}, nm (ν_{max}, cm^{-1})	Difference $\Delta\lambda(_{G-W})$, nm ($\Delta\nu(_{G-W})$, cm^{-1})	
	shape λ_{max}, nm	shape+size λ_{max}, nm (ν_{max}, cm^{-1})		Calc.	Meas.
Water	358	374 (26738)	393 (25445)		
Glycerol	365	388 (25773)	409 (24450)	14 (965)	16 (995)

26

Table 7. Calculated and experimental value obtained for the peak position of spectra $\varepsilon_2^{meso}(\nu)$ for Au nanoboxes of different size impregnated into two different matrices (water and glycerol).

Matrix	Calculations		Measurement λ_{max}, nm (ν_{max}, cm^{-1})	Difference $\Delta\lambda$(G-W), nm ($\Delta\nu$(G-W), cm^{-1})	
	shape λ_{max}, nm	shape+size λ_{max}, nm (ν_{max}, cm^{-1})		Calc.	Meas.
Water	597	724 (13812)	724 (13812)		
Glycerol	624	775 (12903)	760 (13158)	51 (909)	36 (654)

Table 8. Calculated and experimental value obtained for the peak position of spectra $\varepsilon_2^{meso}(\nu)$ for Au spherical particles (diameter 2.5 nm) impregnated into two different matrices (water and glycerol).

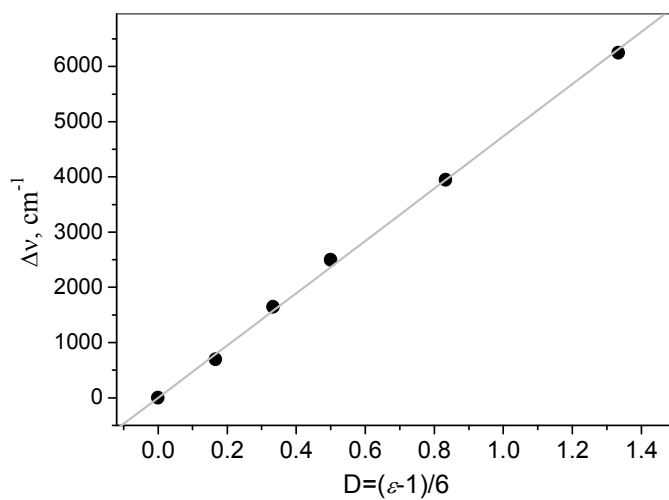| Matrix	Calculations		Measure-ment λ_{max}, nm (ν_{max}, cm^{-1})	Difference $\Delta\lambda_{(G-W)}$, nm ($\Delta\nu_{(G-W)}$, cm^{-1})	
	shape λ_{max}, nm	shape+size λ_{max}, nm (ν_{max}, cm^{-1})		Calc.	Meas.
Water	536	536 (18657)	535 (18692)		
Glycerol	548	548 (18248)	541 (18484)	12 (409)	6 (208)

Figure Captions

Figure 1.   Dependence of the inductive-resonant shift of gold plasmon frequency versus dielectric constant of a surrounding matrix in quasistatic approximation.

Figure 2. TEM images and UV-VIS spectra of Ag nanoprisms with different height of particles triangular face: (a,b) – 23 nm, (c,d) – 20.6 nm, (e,f) – 13.8 nm. Solid lines – experimental absorption spectrum of nanoprisms diluted in aqueous solution (black line) and in glycerol (orange line). Short dot lines – calculated absorption spectra using Eq. (23) for ε_h=1.777 (black dots) and ε_h= 2.17 (orange dots).
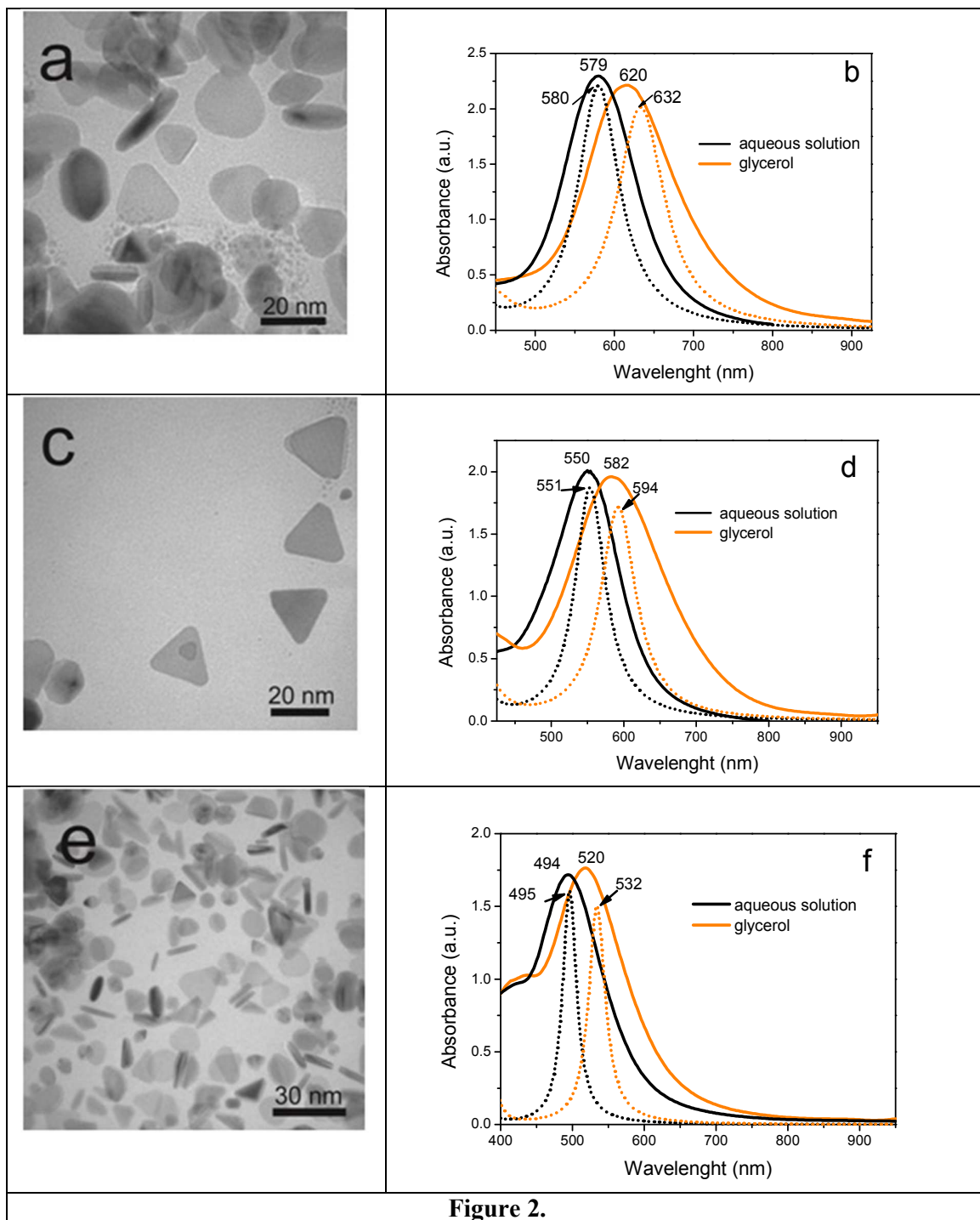
Figure 3. a) TEM images and b) UV-VIS spectra of Ag nanowires with size of 15.8 nm. In figure (b): solid lines – experimental absorption spectrum of nanowires diluted in aqueous solution (black line) and in glycerol (orange dotted line). Short dot lines – calculated spectra using Eq. (23) for ε_h=1.777 (black dots) and ε_h= 2.17 (orange dots).
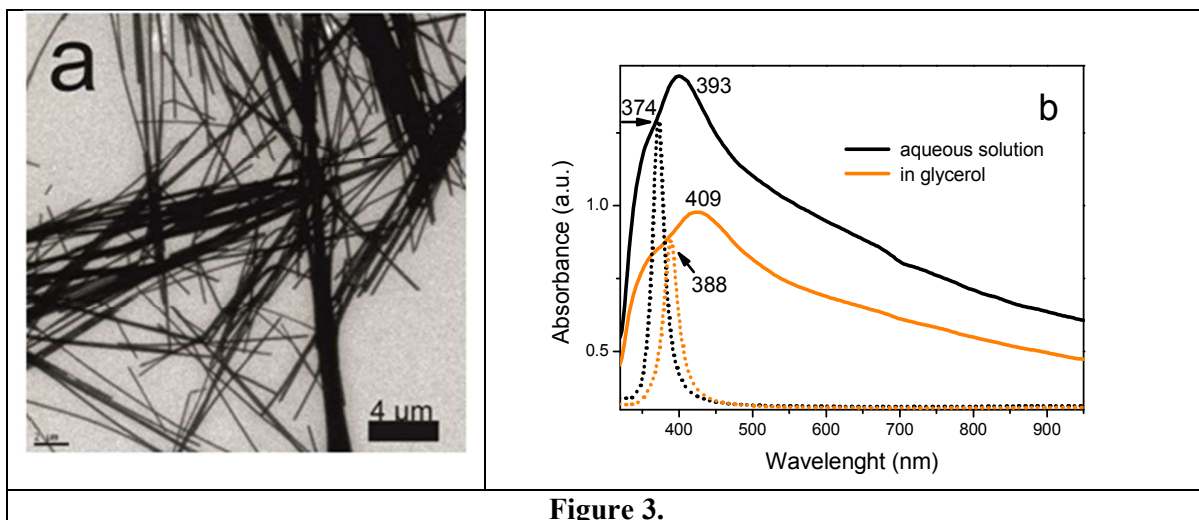
Figure 4. TEM images and UV-VIS spectra of Au nanoparticles: (a,b) – nanoboxes with size 64 nm, and (c,d) – nanospheres with size 2.5 nm. In figures (b) and (d): solid lines – experimental absorption spectrum of Au nanoparticles diluted in aqueous solution (black line) and in glycerol (orange line). Short dot lines – calculated spectra using Eq. (23) for ε_h=1.777 (black dots) and ε_h= 2.17 (orange dots).

28

Figures to paper: "Influence of intermolecular interactions on spectroscopic characteristics of metal nanoparticles and their composites" by Igor I. Shaganov, Tatiana S. Perova, Maria V. Mukhina, Irina V. Martynenko, Alexander V. Baranov, Anatoly V. Fedorov, Valerie Gerard and Yuri K. Gun'ko
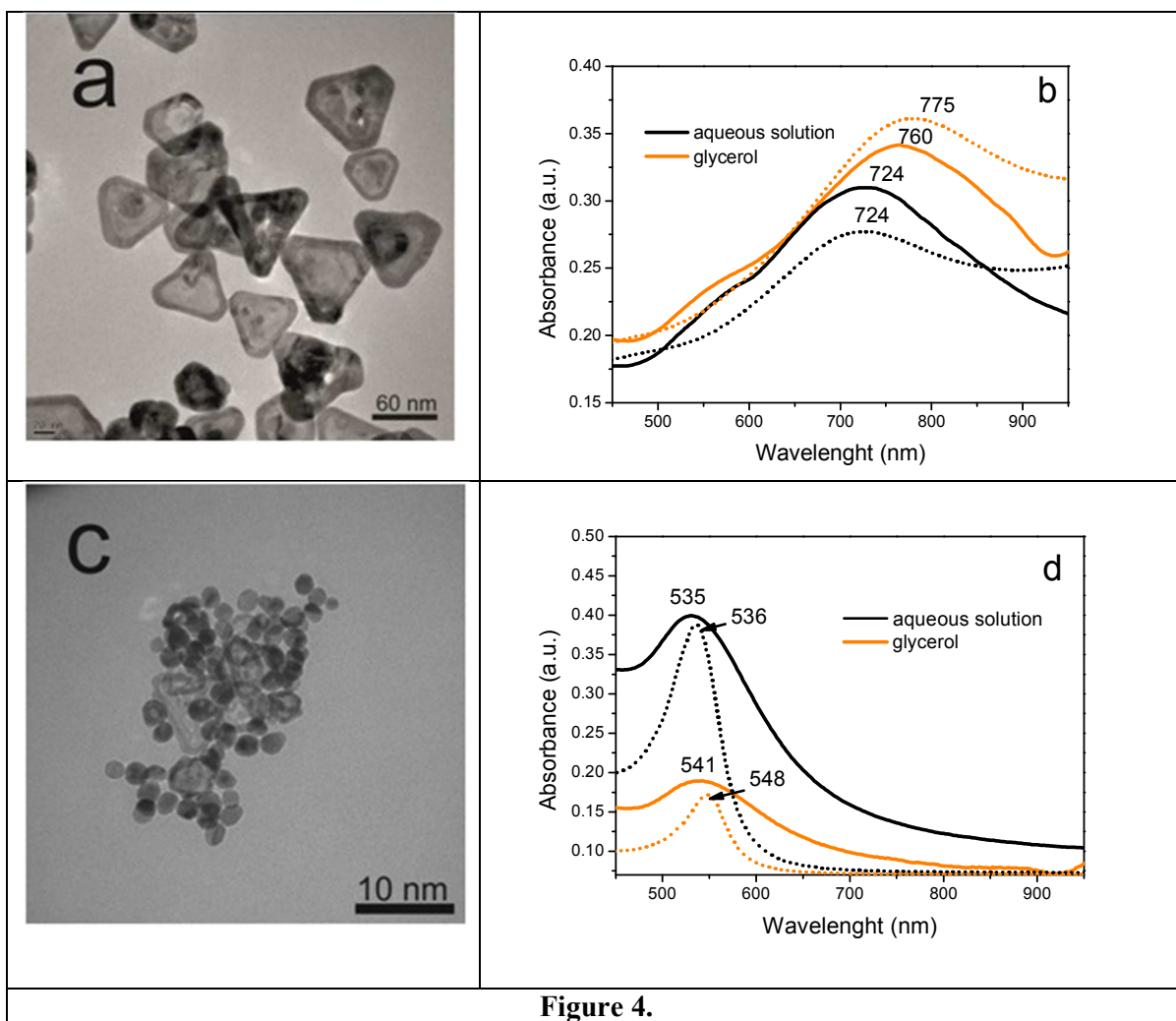

Figure 1.

Figure 2.

Figure 3.

Figure 4.